2020

An Experimental Validation of a Revised Paschen's Law Relating to the ESD of Aerospace Vehicle Surfaces

Manuela Morales
University of Central Florida

AN EXPERIMENTAL VALIDATION OF A REVISED PASCHEN'S LAW RELATING TO THE ESD OF AEROSPACE VEHICLE SURFACES

by

MANUELA MORALES

A thesis submitted in partial fulfillment of the requirements for the degree of Bachelor of Science in the Department of Mechanical Engineering in the College of Engineering and Computer Science at the University of Central Florida Orlando, Florida.

Spring 2020

Thesis Chair: Kareem Ahmed

ABSTRACT

The experimental validation of a new theoretical model of Paschen's law was developed. In order to do so, a supersonic wind tunnel apparatus was designed to induce electrostatic discharge between two electrodes. Tests are conducted at different sub-atmospheric pressures, electrode gap distances and under supersonic test conditions. This was possible using interchangeable nozzle and test sections. The wind tunnel included the implementation of an automated recording of current and voltage data via a LabVIEW™ program collected relevant data, which once analyzed, was used to support the revised Paschen Law developed by Dr. Houge et.al. Results showed that the modified Paschen's law is consistent with experimental results. However, by analyzing the experimental data, it was noted that further work is needed because additional parameters, such as relative humidity, need to be considered.

TABLE OF CONTENTS

LIST OF FIGURES

CHAPTER ONE: INTRODUCTION

The Journal of Electrostatics defines electrostatics as "phenomena resulting from the interaction of stationary or moving electrical charges, where the interaction is due solely to the charges and their positions and not due to their motion" [1]. It is relevant in many fields, but for the purpose of this research, a focus is placed in the area of aerospace systems. It can affect the design, manufacturing, performance and other aspects of a product or process. An important law in the field of electrostatics is Paschen's Law, developed by Friedrich Paschen in 1889. This law relates voltage behavior over small gap distances between electrons in a gas medium. Essentially, the law states relate voltage behavior over small gap distances between electrons in a static gas medium. Essentially, as voltage is increased, an electric potential is built up between electrodes. Particles, due to their natural charge, separate and move towards oppositely charged electrode. During this process, there is the possibility that particles clash with each other, building a bridge of charged particles that lead to an electrostatic discharge. Paschen's law can mathematically explain this behavior yet it is limited by the fact that such law only fully applies when a static medium is presented. Paschen's law is of great importance in different industries around the world. Thanks to Paschen's Law, for example, when a maintenance worker must work near or with high voltages, safe distances have been established for them to work outside of objects which can induce high voltage electrostatic discharge conditions. As mentioned before however, this research focuses in the aerospace industry. When it comes to designing for example a rocket, Paschen's Law is utilized to determine a safe distance where equipment such as antennas and onboard computer systems that collect data, are appropriately located within the aerospace vehicle.

However, this may change once the rocket is launched, now, a dynamic medium is present as air is flowing through.

In today's aerospace developments and applications, Paschen's Law, if modified to consider gas velocity, can lead to several benefits to the scientific community. In collaboration with Dr. Michael Hogue, from NASA's Electrostatics & Surface Physics laboratory, a couple concerns of electric discharge in a dynamic medium have been expressed, especially in regard to re-entry vehicles travelling at supersonic speeds. Aerospace vehicles whose surfaces may be triboelectrically charged, meaning certain materials become electrically charged after they are separated from a different material with which they were in contact, by dust or ice crystal impingement while traversing the atmosphere. Revising Paschen's Law and applying dynamic medium conditions, scientists will be able to evaluate different atmospheric and sub-atmospheric conditions, leading to the prevention of electrostatic discharges (ESDs). This can potentially enhance the safety of aerospace vehicles through a redefinition of electrostatic launch commit criteria.

Previous research has been done in the subject by Hogue [2], along with others from NASA's Electrostatics and Surface Physics Laboratory (ESLP).The purpose of their work was to "develop a version of Paschen's Law that takes into account the flow of ambient gas past electrode surfaces" [2] . Their research has highlighted that by mitigating ESD, the electrostatic criteria during launch aborts can be modified, saving millions of US dollars in overhead. Additionally, better anti-static coatings can be developed for use in the industry.

The purpose of this project is to experimentally validate a theoretical model of a modified Paschen's law [3] developed previously in a Science Innovation Fund (SIF) NASA project [2]. In order to do so a supersonic wind tunnel apparatus will be designed and fabricated to voltage discharge between two electrodes at different pressures and distances. This wind tunnel will include implementation of an automated recording of current and voltage data via a LabVIEW™ program that will collect relevant data, which once analyzed, will be used to support the revised Paschen Law developed by Dr.Houge et.al. The proposed project is in collaboration with NASA Kennedy Space Center. The project aligns with two of NASA's strategic goals. First, Objective 1.1, which seeks to expand human presence into the solar system and to the surface of Mars to advance exploration, science, innovation, benefits to humanity, and international collaboration. Secondly, Objective 1.3, which seeks to Facilitate and utilize U.S. commercial capabilities to deliver cargo and crew to space [4]. NASA's Technology Roadmap TA 13.3.2 Environment-Hardened Materials and Structure is directly related as well. Given that this project will help further understand the electrical breakdown in a supersonic flow, results can potentially help develop mitigation strategies and products [4] related to electrostatic engineering development.

The proposed project also relates to two of Kennedy Space Center's five core competencies that classify this idea as a precursor to additional beneficial work to the organization. They are: (1) Designing, developing, operating, and sustaining flight and ground systems and supporting infrastructure and (2) Development, testing, and demonstration of advanced flight systems and transformational technologies to advance exploration and space systems [5].

CHAPTER TWO: SELECTED LITERATURE REVIEW

Cotton, A. Nelms and M. Husband, "Defining safe operating voltages for aerospace electrical systems," 2007 Electrical Insulation Conference and Electrical Manufacturing Expo, Nashville, TN, 2007.

This publication explores the systems used in high voltage operations to transmit power in an aircraft. As aircraft design improves, reliability on the implementation of electrical technology increases. More aircraft operations such as de-icing systems or electrical flight control actuation depend on this. Cotton et.al [7], explain that by adding these systems to the aircraft cable weights and issues related to voltage drop increase in number. By using higher voltages to reduce weight from cables, a higher likelihood of electrical discharge comes along. During this study, Cotton.et al studied such voltages to determine when can they be used without partial electric discharges. This study is done from a theoretical standpoint, supported on previous experimental results. The study leads to conclude that “an increase to ever higher voltages does not lead to a continuous reduction in the power transfer to weight ratio of cabling systems.” Cotton’s work can be used to explore the possible challenges faced when replacing mechanical and electrical aircraft systems at higher voltages.

Melnik, Olga, and Michel Parrot. "Electrostatic discharge in Martian dust storms." Journal of Geophysical Research: Space Physics 103.A12 (1998)

This publication explores the possibility of electrical discharge in the Martian atmosphere. Melnik and Parrot [8] explain this could happen due to dust masses getting electrically charged during large dust storms. Atmospheric pressures on planets such as Mars requires a lower voltage

value to generate electrical discharge when compared with Earth. Through experimentation and numerical simulation, Melnik and Parrot were able to further understand these conditions. Utilizing Poisson's equation and the continuity, the electrostatic potential and evolution of charge density were calculated. Results lead to a set of specific conditions for electric discharge to occur.

Sickafoose, A. A., et al. "Experimental investigations on photoelectric and triboelectric charging of dust." Journal of Geophysical Research: Space Physics 106.A5 (2001)

These experimental investigations were "pertaining to the charging of single dust particles in space due to three effects: (1) photoemission, (2) the collection of electrons from a photo emissive surface, and (3) triboelectric charging." [9] Results from experimentation show that for silicate planetary regolith analogs, the dominant charging process is triboelectric. The relevance regarding this research lays on various points such as electromagnetic forces that sculpt dust rings and electromagnetic dust levitation and transport in lunar and Martian surfaces. Sickafoose et.al [8] highlights the effect these such electromagnetic forces can affect the dynamics of turbulent flows in the near-surface boundary layer, due to effects from the photoelectron layer. By understanding how dust particles in the surface get electrically charged, the evolution of planetary surfaces and dust rings can be further studied. Sickafoose et.al [9] can introduce the importance of considering a dynamic gas medium. Given that dust particles can be electrically charged by friction of two nonconductive objects, or triboelectrically charged, it means that when an aerospace vehicle is in flight, and crosses the earth's atmosphere, it may be triboelectrically charged. If this happens, ESD could occur, generating damage to the vehicle and opening doors to possible in-flight difficulties.

Hogue, M. D., Cox, R. E., Mulligan, J., Kapat, J., Ahmed, K., Wilson, J. G., & Calle, L. M. (2017). Revision of Paschen's Law Relating to the ESD of Aerospace Vehicle Surfaces.

Hogue et.al [10] developed a revision of Paschen's Law where dynamic gas flow is accounted for in partnership with the Center for Advanced Turbomachinery & Energy Research (CATER) at UCF. In 2010, as a result of an electrostatic safety analysis made on the Ares I rocket, safety of the flight termination system (FTS) housing against triboelectric charging was seen [10]. This analysis was performed by the Electrostatics and Surface Physics Laboratory (ESPL) at the Kennedy Space Center (KSC). Data collected from this showed to be consistent with the revised Paschen's Law. Hogue mentions that the designed test facility could only reach a small window of pressures, therefore limiting the range of validation. Additionally, due to the electrode introduced in the flow, undesired shock reflections existed, creating untrustworthy pressure values. During the experimentation process, two pressure transducers where placed in the facility, one upstream from the electrode and one downstream from the electrode. When a shock reflection is present, a pressure increase occurs. This means that the pressure recorded downstream would not match the pressure recorded upstream. Therefore, this project seeks to do such validation under ideal flow conditions, and a wider pressure range.

CHAPTER THREE: THEORICAL BACKGROUND

Paschen's law defines the relationship between the discharge voltage of two electrodes in a static gas medium as a function of the gas's stagnation pressure and the distance between electrodes. This law can be seen below:

$$\boldsymbol{Vs} = \frac{\frac{\boldsymbol{V_i}}{\boldsymbol{LP_{atm}}}(\boldsymbol{Pd})}{\boldsymbol{ln}(\boldsymbol{Pd}) - \boldsymbol{ln}\left[\boldsymbol{LP_{atm}}\boldsymbol{ln}\left(\mathbf{1} + \frac{\mathbf{1}}{\boldsymbol{y}}\right)\right]} \quad \textbf{(1)}$$

Here, *Vs* stands for sparking discharge voltage, *Vi* is ionization potential of the ambient gas, *L* is molecular mean free path at standard atmospheric pressure, *Patm* is atmospheric pressure at sea level, *P* is total gas pressure, *y* is secondary electron emission coefficient, *d* is electron separation and Prior to further explain the nature of the current research, it is helpful to revise some of the previous work done by Hogue to better understand today's stance. Initially, Hogue states that the revised Paschen Law must reduce to the original Paschen Law equation when velocity is zero, the following equation is developed:

$$\boldsymbol{Vs} = \frac{\frac{\boldsymbol{V_i}}{\boldsymbol{LP_{atm}}}(\boldsymbol{Pd})}{\boldsymbol{ln}(\boldsymbol{Pd}) - \boldsymbol{ln}\left[\boldsymbol{LP_{atm}}\boldsymbol{ln}\left(\mathbf{1} + \frac{\mathbf{1}}{\boldsymbol{y}}\right)\right] - \boldsymbol{M}} \quad \textbf{(2)}$$

Here, *M* is Mach number. By having a Mach number of zero, the equation reverts to the original Paschen law. Through several iterations, Hogue took consideration of dynamic pressure, leading to a final version of the revised law seen below:

$$Vs = \frac{\frac{V_i}{LP_{atm}}\left(1 + \frac{\gamma_a - 1}{2}M^2\right)^{\frac{\gamma_a}{\gamma_a - 1}}(Pd)}{ln\left[\left(1 + \frac{\gamma_a - 1}{2}M^2\right)^{\frac{\gamma_a}{\gamma_a - 1}}\right] - ln\left[LP_{atm}ln\left(1 + \frac{1}{y}\right)\right] - M} \quad \textbf{(3)}$$

CHAPTER FOUR: FACILITY DESIGN

The outlined research is being conducted at the Propulsion and Energy Research Laboratory (PERL) at the University of Central Florida (UCF). The test facility consists of three main sections: an inlet, an expansion and a test section as shown in Fig 3. The materials used are stainless steel, T6-6061 aluminum, polycarbonate, and acrylic.

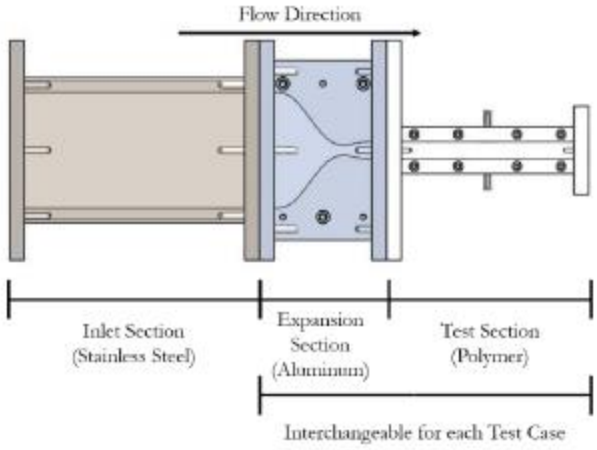

Figure 1. Side view of experimental facility

To collect a variety of data, four different converging-diverging (CD) nozzles were fabricated. This means the expansion section and test sections are interchangeable depending of the desired Mach number and gap distance being evaluated. Mounted to the test sections, custom designed electrodes were placed at desired gap distances. These electrodes transmit a voltage from a power supplied attached to the tunnel. The design of the electrodes is specific to avoid shock waves inside the test section.

The following calculations were used in the design of the supersonic facility:

- The design of the CD nozzles was done using a method of characteristics used to produce desired Mach values of 1.5 and Mach 2 flow. The nozzle area ratio formula was calculated using the isentropic flow relation [10], and can be seen below:

$$\frac{Ae}{A^*} = \frac{1}{Me}\left[\left(\frac{2}{\gamma_a + 1}\right)\left(1 + \frac{\gamma_{a-1}}{2} {M_e}^2\right)\right]^{\frac{\gamma_a+1}{2(\gamma_a-1)}} \quad (4)$$

Using these calculations, the plots of the nozzle contours below were found:

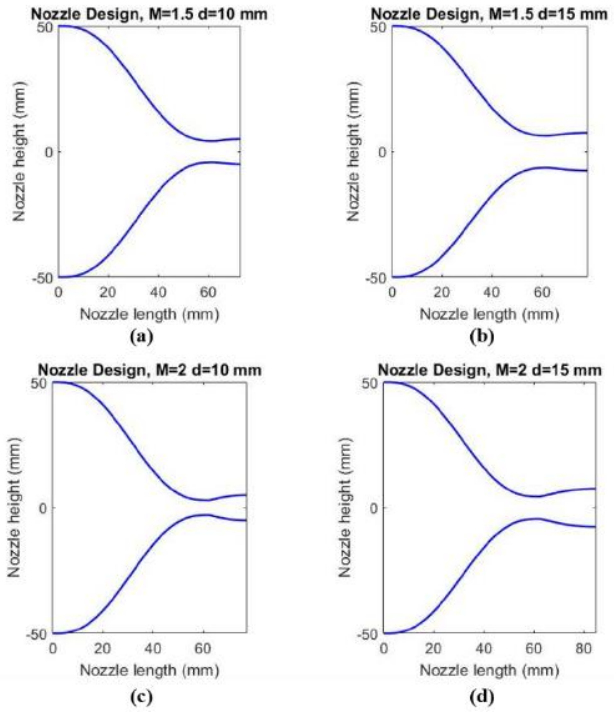

Figure 2. CD Nozzle contours

- Flowing fluids have two components relevant to this project: stagnation pressure (P) and static pressure (Pa). A desired pressure range was specified in order to have the flow ideally expand to obtain atmospheric pressure in the test section. To achieve this, the required stagnation pressure was found through the isentropic flow relation [11] and its equation is seen below:

$$\frac{P}{P_a} = (1 + \frac{\gamma_a - 1}{2} M^2)^{\frac{\gamma_a}{\gamma_a - 1}} \quad (5)$$

The plots below show the expected pressure range from the calculations at two different distances:

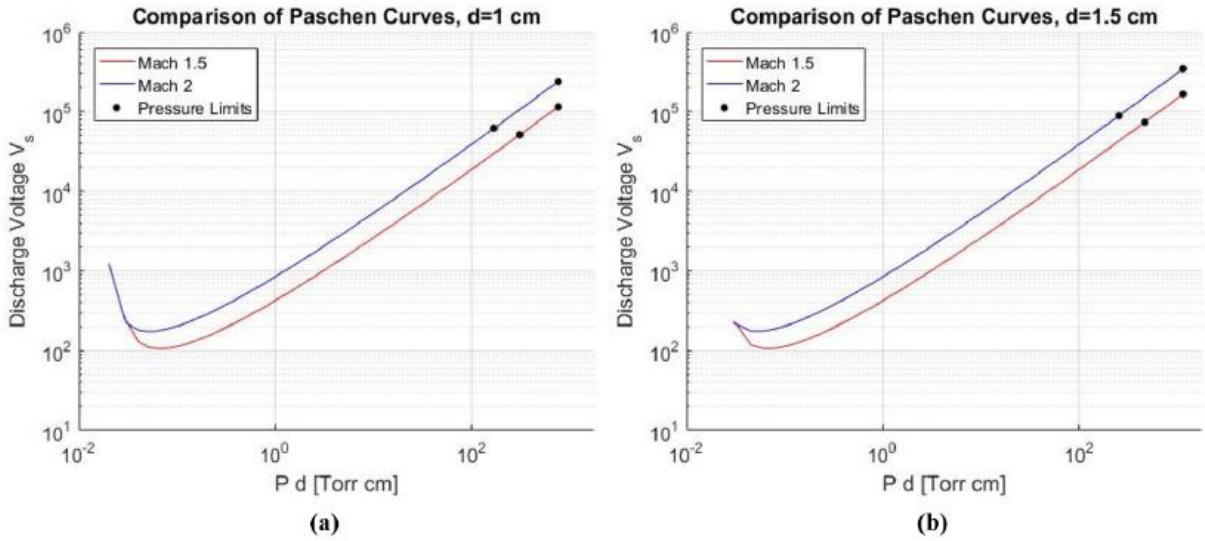

Figure 3. Expected pressure range at a) 1 cm electrode gap and b) 1.5 cm electrode gap

- Once the stagnation pressure was found, it was used to define the minimum test section static pressure for each case. The formula is seen below:

$$\frac{P_{atm}}{P_a} = \frac{2\gamma_{aM^2}}{\gamma_{a+1}} - \frac{\gamma_a - 1}{\gamma_a + 1} \quad (6)$$

CHAPTER FIVE: EXPERIMENTAL PROCEDURE

As stated before, previous experimentation was done with CATER and ESPL. In this work, a custom electrode was inserted into a supersonic wind tunnel and charged by a Glassman 60 kV power supply. The test procedure consisted of a power supply voltage ramped up until discharge occurred at steady state flow. Discharge voltage and discharge pressure were then recorded in LabView. A Schlieren system along with a go-pro where put in place for image collection. The schematic below summarizes the described set up:

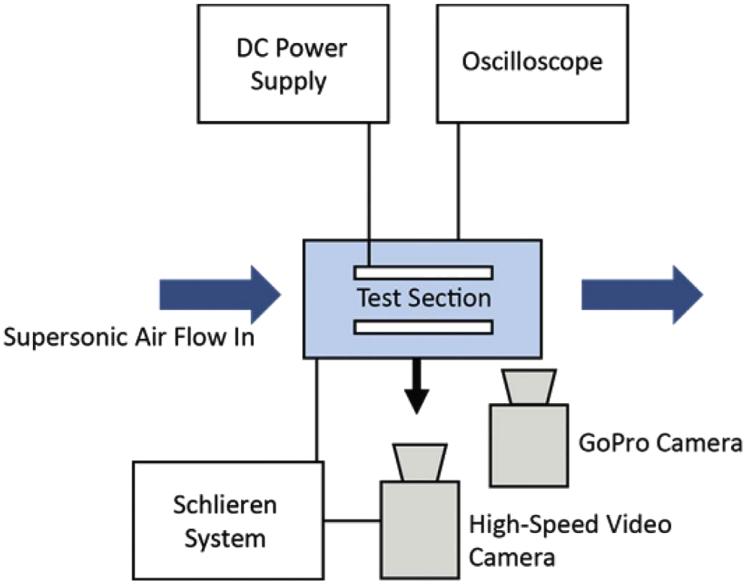

Figure 4. Previous experimental facility set up

During experimentation, the supersonic steady state condition only lasted for 30 seconds or less, depending on the air tank pressure and the Mach number. This made it difficult to ramp the electrode voltage in such a short a time. Also, the pressure between the electrode and the upper

surface of the test section was not fully consistent across the electrode because of shock reflections caused by an intrusive electrode. The Schlieren image in Fig 2 helps illustrate this:

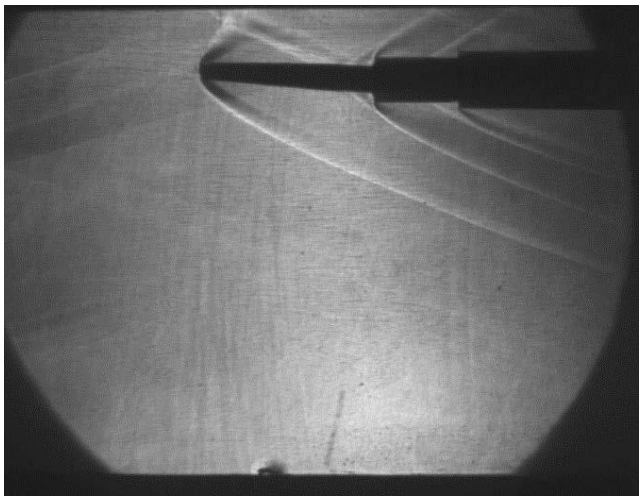

Figure 5. Previous experimental facility set up [10]

Although the experimental results to date are consistent with the hypothesis, more data is required. A follow-on experiment was proposed, which leads to the current research.

The study consists of air from 32 48- liter tanks pushed through a constant area inlet, into the CD nozzle until a steady state is reached. Once this occurs, the electrodes mounted in the test section, which are charged through a Glassman 60kV Series EH power supply, have their voltage progressively increased from 0 to 50 kV until discharge occurs. A LabVIEW™ program is connected to pressure transducers and the power supply. Once the discharge occurs, the power supply is shut off and pressure and voltage values are recorder. Additionally, Schlieren images of supersonic shock waves are collected using a Photron AQ1.1 high speed camera. This procedure

is repeated at different desired pressures, Mach numbers and gap distances. The flowchart of the experimental procedure is seen in Fig 6.

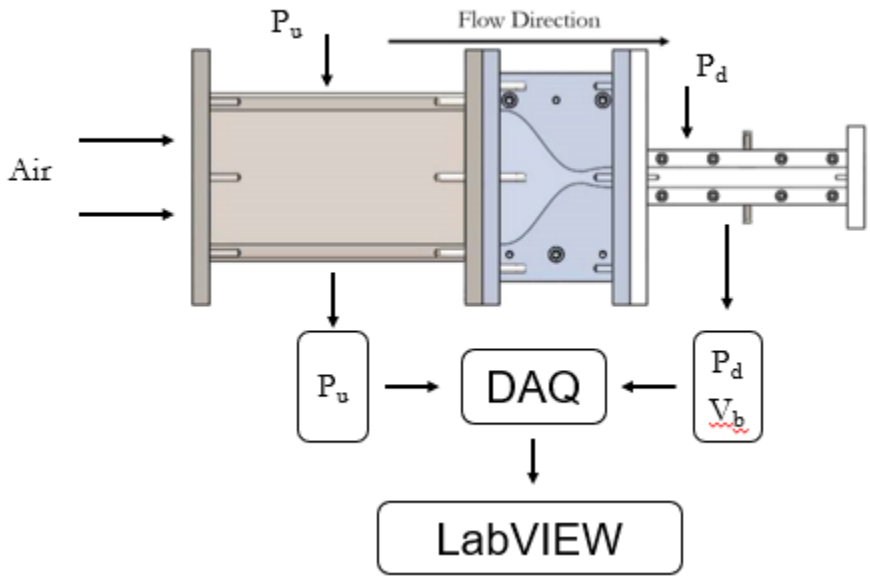

Figure 6. Flowchart of experimental procedure

The values selected to run the facility were to target supersonic conditions in which aerospace vehicles. Two electrode gap sizes and various sub-atmospheric pressures to validate the modified Paschen law discharge curve. The targeted test conditions are seen in Fig 7.

Test Case	Mach Number	Gap Distance (mm)	Min Static Pressure (Torr)	Max Static Pressure (Torr)
1	1.5	10	309.15	760
2		15		
3	2	10	168.89	
4		15		

Figure 7. Targeted Test conditions

CHAPTER SIX: RESULTS

So far, experimentation has occurred for Mach number 2. Data collected was analyzed using MATLAB and figure 8 was produced.

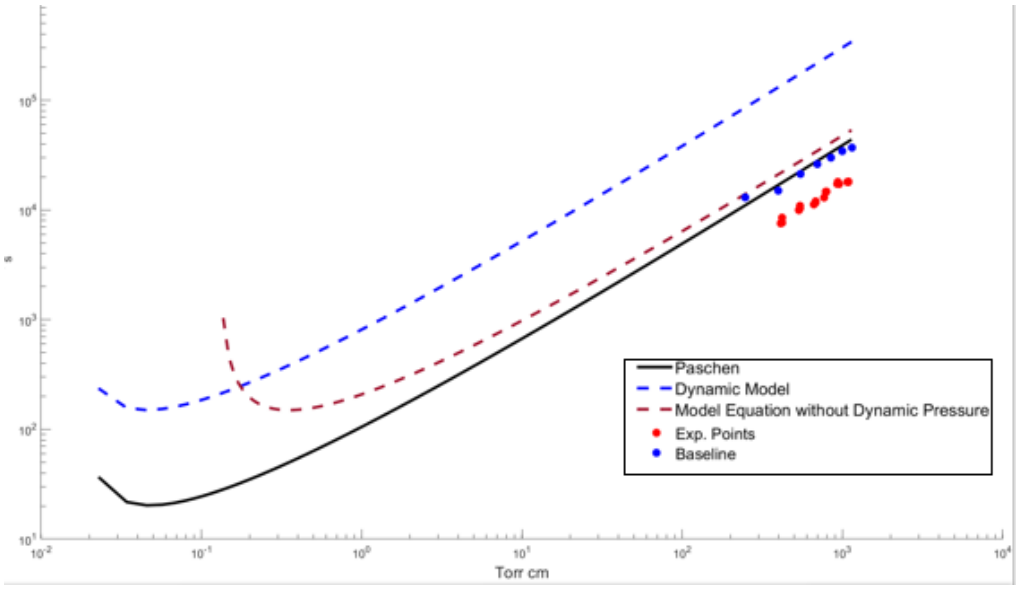

Figure 8. Experimental data and proposed model

Here it can be observed that the experimental data points are quite far off from the proposed model. Calculations were made (See Appendix I) and the equation that takes account dynamic pressure had an average margin of error of 94.3%. The equation that did not consider dynamic pressure however, showed a lower margin of error, being 70.5% the average. This feedback was sent to Hogue and as a response two new possible equations, where relative humidity (H) was considered, were produced:

Version A:

$$V_s = \frac{\frac{V_i}{LP_{atm}}(Pd)H}{ln(Pd) - ln\left[LP_{atm}ln\left(1+\frac{1}{\gamma}\right)\right] - M} \quad \textbf{(7a)}$$

Version B:

$$V_s = \frac{\frac{V_i}{LP_{atm}}(Pd)H}{ln(Pd) - ln\left[LP_{atm}ln\left(1+\frac{1}{\gamma}\right)\right] - M + H} \quad \textbf{(7b)}$$

The data plotted against these two new equations is seen in figure 9.

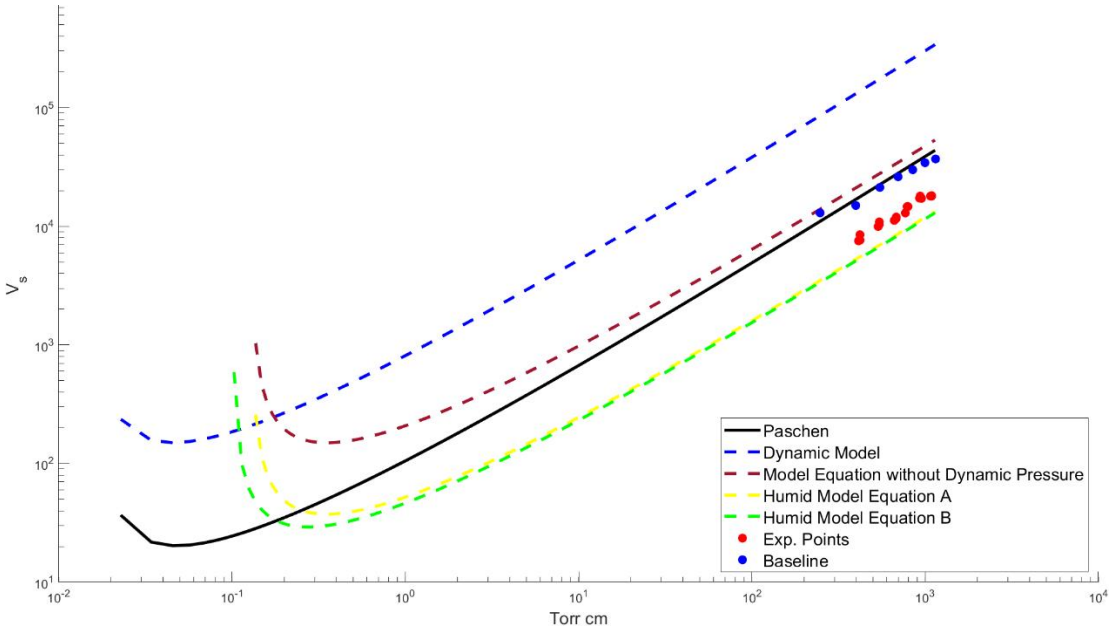

Figure 9. Experimental data and new proposed equations

Here, we see that the new proposed models align closer to the experimental points. In this case, equation A had an average margin of error of 21.9% while equation B had a lower percentage, this being 17.7%. From this data, it is correct to assume that so far, equation B aligns best with the experimental points. The reasoning behind this lies on a new hypothesis proposed by Hogue; as relative humidity is increased; a lower discharge voltage should be seen. Equations A and B were calculated at a 46% humidity, correspondent to the humidity from the testing day. If, theoretically, the relative humidity is lower to 25%, equations B's voltages increase, and equation A's voltages

decrease. This means equation B best aligns to the hypothesis that relates sparking voltage and relative humidity. While it is still not perfectly aligned, efforts are continued to find and equation that has a lower margin of error.

From the results it is also important to highlight the role of pressure and ESD behavior. The higher the pressure is, the higher the discharge voltage is. This means that pressure should have an inversely proportional behavior with relative humidity.

To further validate our findings, a velocimetry analysis was performed using the Schlieren images taken during the experimental procedure. Schlieren imaging was necessary to observe that the shockwave generated from flow did not influence the ESD measurements over the electrodes. By measuring velocity through the images, it is possible to assess how much of a uniform Mach number is the flow. Using MATLAB and a method approach based off the one seen on Morales [12], Schlieren images were converted to binary images in MATLAB. Based on their intensities, different regions were masked, and their centroids were found. Visually inspecting the movement of pixels, a correlation was created, and the Euclidean distance was found using the formula below:

$$\boldsymbol{D_{xy} = \sqrt{(x_{(i+1)} + x_i)^2 + (y_{(i+1)} + y_i)^2}} \quad \textbf{(8)}$$

The velocity is then obtained by using the distance of the test section as a calibration to find equivalence between pixels and meters and taking into account the camera frame rate.

A sample pair of pixels analyzed is seen below:

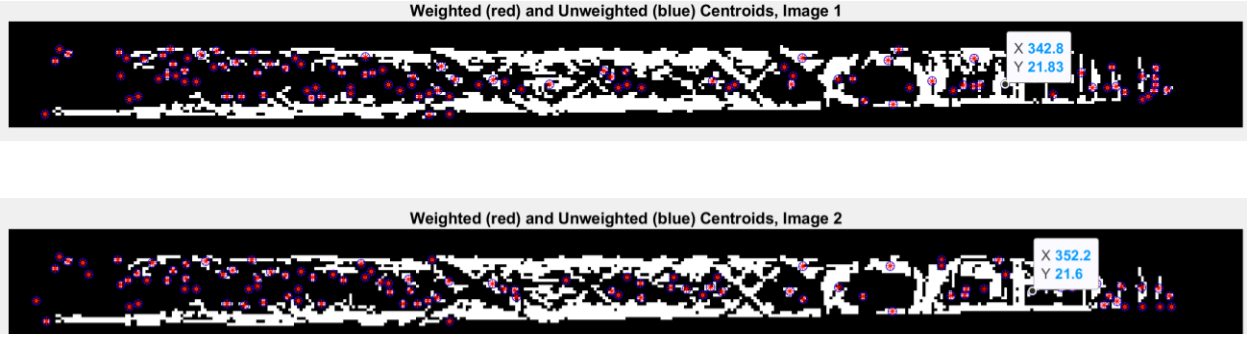

Figure 10. Two centroid locations from Binary Schlieren Images from MATLAB

With the pixel locations noted in Figure 10, along with a conversion to meters per second based on a camera frame rate of 18,000 fps, the velocity found was that of 661.73 m/s, correspondent to around 1.9 Mach. This method needs to be further developed in order to apply it to all pixels and find a correlation between them to evaluate the assertiveness of pixel pairs selected across different frames.

CHAPTER SEVEN: CONCLUSION AND FUTURE WORK

The work presented in this thesis can show that voltage behavior over small gap distances between electrons in a static gas medium differs significantly from that of a dynamic medium. Figures 8 and 9, along with data from Appendix I show that the experimental data is far off from the original Paschen curve. There is a 55.5% margin of error between the discharge voltages from a static medium versus a dynamic medium. This highlights the importance in the need for a revised law that considers a dynamic medium as it could potentially reduce the threshold of electrostatic launch commit criteria.

Additionally, while experimental data supports initial hypothesis proposed by Hogue, it has been discovered through this research that in order to revise Paschen's law and apply it to a dynamic gas medium, other parameters besides Mach number, such as relative humidity, affect the behavior of gases. Based on the results, equation B seems to be the best fit so far to model the behavior of the experimental points, and it obeys the hypothesis proposed by Hogue

It is also possible to conclude that the re-design of the electrode, avoids the shock generation found in previous experimentation providing cleaner and reliable data. It is also possible to sustain this by looking at the velocimetry analysis performed on Schlieren images, were it is possible to confirm that the Mach number desired is present in the test section.

Future work for this research includes the further development of the Schlieren Image Velocimetry (SIV) presented along with experimental data collection for the remaining Mach cases. Data will be sent to Hogue and the final equation that shall relate voltage behavior over small gap distances between electrons in a dynamic medium will continue to be developed.

REFERENCES

[1] Lacks, D. “Journal of Electrostatics.” Elsevier, www.journals.elsevier.com/journal-of-electrostatics.

[2] M. Hogue, et. al., “Dynamic Gas Flow Effects on the ESD of Aerospace Vehicle Surfaces”, SIF final report, December, 2016.

[3] F. Paschen, Wied. Ann., 37, 69, (1889).

[4] NASA Strategic Plan 2014. http://www.nasa.gov/sites/default/files/files/FY2014_NASA_SP_508c.pdf.

[5] 2015 NASA Technology Roadmap. http://www.nasa.gov/offices/oct/home/roadmaps/index.html.

[6] Ground and Launch Systems Processing Roadmap, Technology Area 13, NASA KSC, April, 2012.

[7] Cotton, A. Nelms and M. Husband, "Defining safe operating voltages for aerospace electrical systems," 2007 Electrical Insulation Conference and Electrical Manufacturing Expo, Nashville, TN, 2007.

[8] Melnik, Olga, and Michel Parrot. "Electrostatic discharge in Martian dust storms." Journal of Geophysical Research: Space Physics 103.A12 (1998)

[9] Sickafoose, A. A., et al. "Experimental investigations on photoelectric and triboelectric charging of dust." Journal of Geophysical Research: Space Physics 106.A5 (2001)

[10] Hogue, M. D., Cox, R. E., Mulligan, J., Kapat, J., Ahmed, K., Wilson, J. G., & Calle, L. M. (2017). Revision of Paschen's Law Relating to the ESD of Aerospace Vehicle Surfaces.

[11] John, J. E., & Keith, T. G. (2006). Gas Dynamics. Upper Saddle River: Pearson Prentice Hall.

[12] Morales, Rudy. “Lagrangian Schlieren Image Velocimetry Measurements in Exhaust Plumes.” New Mexico Institute of Mining and Technology, 2018

APPENDIX 1

Target Pressure [Torr]	Test Number	Measured Pressures [Torr]	Measured Voltages [kV]	Paschen Voltage [kV]	Modified Paschen with Dynamic Pressure [kV]
260	1	274.99	7.545	17.442	135.70
	2	279.59	7.338	17.704	137.75
	3	280.14	8.495	17.735	137.99

360	1	356.78	9.965	22.059	171.65
	2	362.34	10.899	22.369	174.06
	3	362.18	10.352	22.360	173.99
460	1	453.27	11.663	27.390	213.15
	2	453.90	11.968	27.424	213.42
	3	442.25	11.231	26.786	208.45
560	1	530.08	14.695	31.564	245.66
	2	529.74	12.856	31.545	245.51
	3	512.35	12.963	30.605	238.91
660	1	634.99	17.224	37.184	289.42
	2	617.27	17.098	36.240	282.08
	3	623.50	18.002	36.572	284.66
760	1	692.92	17.324	40.254	313.34
	2	715.38	17.992	41.438	322.56
	3	698.79	16.557	40.564	315.75

Modified Paschen without Dynamic Pressure [kV]	Version A	Version B	Static Discharge Discrepancy	Paschen Discrepancy
26.440	10.012	9.472	-20.4%	-56.7%
26.832	10.183	9.635	-22.6%	-58.6%
26.878	10.176	9.628	-10.4%	-52.1%

33.323	12.584	11.925	5.1%	-54.8%
33.785	12.756	12.090	14.9%	-51.3%
33.772	12.751	12.085	9.2%	-53.7%
41.252	15.541	14.749	23.0%	-57.4%
41.303	15.559	14.767	26.2%	-56.4%
40.355	15.206	14.429	18.4%	-58.1%
47.449	17.848	16.954	55.0%	-53.4%
47.421	17.690	16.803	35.6%	-59.2%
46.026	17.318	16.448	36.7%	-57.6%
55.780	20.946	19.917	81.6%	-53.7%
54.382	20.463	19.455	80.3%	-52.8%
54.874	20.610	19.595	89.8%	-50.8%
60.326	23.287	22.157	82.7%	-57.0%
62.078	23.608	22.465	89.7%	-56.6%
60.784	23.575	22.433	74.6%	-59.2%

Modified Paschen with Dynamic Pressure Discrepancy	Modified Paschen without Dynamic Pressure Discrepancy	Version A Discrepancy	Version B Discrepancy
-94.4%	-71.5%	-24.6%	-20.3%

-94.7%	-72.7%	-27.9%	-23.8%
-93.8%	-68.4%	-16.5%	-11.8%
-94.2%	-70.1%	-20.8%	-16.4%
-93.7%	-67.7%	-14.6%	-9.8%
-94.1%	-69.3%	-18.8%	-14.3%
-94.5%	-71.7%	-25.0%	-20.9%
-94.4%	-71.0%	-23.1%	-19.0%
-94.6%	-72.2%	-26.1%	-22.2%
-94.0%	-69.0%	-17.7%	-13.3%
-94.8%	-72.9%	-27.3%	-23.5%
-94.6%	-71.8%	-25.1%	-21.2%
-94.0%	-69.1%	-17.8%	-13.5%
-93.9%	-68.6%	-16.4%	-12.1%
-93.7%	-67.2%	-12.7%	-8.1%
-94.5%	-71.3%	-25.6%	-21.8%
-94.4%	-71.0%	-23.8%	-19.9%
-94.8%	-72.8%	-29.8%	-26.2%